



# Determining In-Situ Stress State by Anelastic Strain Recovery Method Beneath Xiamen: Implications for the Coastal Region of Southeastern China

Chongyuan Zhang<sup>1,2,3</sup> · Weiren Lin<sup>4</sup> · Manchao He<sup>1</sup> · Zhigang Tao<sup>1</sup> · Wen Meng<sup>2,3</sup>

Received: 20 August 2021 / Accepted: 30 April 2022 / Published online: 26 June 2022

© The Author(s), under exclusive licence to Springer-Verlag GmbH Austria, part of Springer Nature 2022

## Abstract

The in-situ stress state in the shallow crust of the coastal region of Southeastern China (CRSC) remains poorly understood. We conducted anelastic strain recovery measurements in a 2 km deep geothermal borehole to investigate the in-situ stress state. Four high-quality granite core samples were employed to successfully estimate the full stress tensors. The results show that the maximum principal stress  $\sigma_1$  is nearly vertical, implying an extensional shallow crust that is controlled by normal faulting. From ~1865 to ~1959 m in depth, the maximum and minimum horizontal principal stresses ( $S_{Hmax}$  and  $S_{hmin}$ ) are 36.1–48.7 MPa and 34.0–38.5 MPa, respectively. Based on the paleomagnetic analysis, the orientation of the maximum horizontal compressive stress  $S_{Hmax}$  is determined as  $N43^\circ \pm 19^\circ W$  and aligned with the subduction direction of the Philippine Sea plate. According to the compiled stress data, the  $S_{Hmax}$  orientations in the CRSC rotate counterclockwise towards the Chinese mainland, which are consistent with those of the earthquake focal mechanisms and regardless of earthquake type, indicating a heterogeneous stress field dominancy in the CRSC. Our findings manifest that there is a lower horizontal compressive stress state in the upper crust in the study region. We also discussed the possible influence of in-situ stress on wellbore stability and fracture propagation in hot dry rock exploration and further quantitatively analyzed the reactivation possibility of natural fractures under different injection pressures. This study will provide scientific data for geodynamic research, fault seismicity, and geothermal development in the region in the future.

## Highlights

- We used the anelastic strain recovery (ASR) method to obtain the in-situ stress state at 2 km depth in Xiamen, Fujian, China, indicating that Xiamen is controlled by normal-faulting stress.
- In ASR experiments, rock mechanics and rock compliance experiments were conducted to help better constrain the in-situ stress state.
- The collision of the Eurasian and Philippine Sea plates controls shallow crustal stress pattern and shows a relatively low horizontal compressive stress state in the coastal region of Southeastern China.
- Implications of in-situ stresses on geothermal resource development were discussed and quantitatively analyzed.

✉ Manchao He  
hemanchao@263.net

✉ Zhigang Tao  
taozhigang@cumtb.edu.cn

<sup>1</sup> School of Mechanics and Civil Engineering, China University of Mining and Technology, Beijing 100083, China

<sup>2</sup> Institute of Geomechanics, Chinese Academy of Geological Sciences, Beijing 100081, China

<sup>3</sup> Key Laboratory of Active Tectonics and Geological Safety, Ministry of Natural Resources, Beijing 100081, China

<sup>4</sup> Graduate School of Engineering, Kyoto University, Kyoto 615-8540, Japan

**Keywords** In-situ stress · Anelastic strain recovery · Extensional stress state · Coastal region of Southeastern China (CRSC) · Geothermal exploration

## 1 Introduction

Knowledge of the stress state in the Earth's crust is crucial for understanding plate driving mechanisms, fault interactions, earthquake occurrences, and unconventional energy development (Wu et al. 2016; Sun et al. 2017; Zhang et al. 2017; Li et al. 2019). Yet, measuring the in-situ stress state at great depths has long been a difficult undertaking. Since the Mesozoic, the South China region has been located at the center of a triangular area surrounded by westward subduction of the Pacific plate, northward subduction of the Indian plate beneath the Eurasian plate, and the collision of the North and South China blocks along the Central China Orogeny (Li et al. 2012; Li et al. 2014). The coastal region of Southeastern China (CRSC, mainly refers to the Fujian Province in this study) is located on the southeastern continental margin of the Eurasian plate, thus implying the frontier of super-convergent tectonism. Therefore, the present-day stress state is likely complex and strong there. This unique tectonic setting makes the study region one of the most seismically active areas in China, including many active faults with NW and NE strikes that cross each other and relatively strong earthquakes that usually occur in the zones where the faults cross (Gao et al. 2009). Focal mechanisms indicate that the orientations of the P axes are N125°E, with an elevation angle of 2°–8°, and a nearly vertical middle axis (Lin et al. 2009), indicating that the crust in the CRSC is horizontally compressed in the NW–SE direction, which is consistent with the subduction orientation of the Philippine Sea plate. World Stress Map data indicate that the CRSC has far fewer available stress indicators of focal mechanisms than Taiwan Island, almost all of which indicate normal and strike-slip faulting stress regimes (Hu et al. 2017; Heidbach et al. 2018). Gao et al. (2009) examined shear wave splitting and concluded that the average fast wave polarization is N109.4° ± 42.6°E, which approximately corresponds to the horizontal principal compressive stress in the CRSC. At the surface, continuous deformation observations (i.e., GPS) demonstrate that the entire South China block moved in a direction of N110°–130°E as a whole, at a speed of 8–11 mm/a and without significant differential movements within the block (Molnar and Gipson 1996; Shen et al. 2000; Zhou et al. 2000; Calais et al. 2003; Zhang et al. 2013), indicating that the South China block may be a relatively rigid block with a uniform motion. Consequently, there appears to be a coupled crust in the CRSC with vertically consistent stress orientations.

Given its unique tectonic setting and complex plate interactions, it is important and necessary to further investigate

the in-situ stress state in the shallow crust of the CRSC to understand whether the Eurasian Plate or the Philippine Sea Plate plays a more important role in the stress state of the region. In addition, the CRSC is one of the most promising geothermal zones and has massive hot dry rock resources formed by extensive Cretaceous magmatic activity. The in-situ stress state plays a crucial role in the response of the rock mass of a high-temperature reservoir to hydraulic stimulation injections and is a key input parameter in geomechanical modeling (Valley and Evans 2019). However, knowledge of the in situ stress state data below 500 m in this region is still missing. Herein, we utilize cores from a geothermal borehole to carry out three-dimensional stress measurements using the anelastic strain recovery (ASR) method (Teufel 1983), which is widely used to investigate in-situ stress in hydrocarbon exploration (Sun et al. 2017) and scientific drilling programs such as the KTB scientific borehole (Wolter and Berckhemer 1989) and International Ocean Discovery Program (IODP) (Lin et al. 2007; Byrne et al. 2009; Yamamoto et al. 2013; Cui et al. 2014; Oohashi et al. 2017; Wang et al. 2020). Hence, this core-based method is a more convenient and effective approach than others for measuring the stress state at depths up to several kilometers (Lin et al. 2006; Sun et al. 2017; Wang et al. 2020).

The JM-1 borehole is located in Xiamen City in southeastern China, which is adjacent to the Zhangzhou Basin and has many high-quality geothermal fields. The JM-1 borehole passes through Pleistocene alluvial sediments, and the Yanshanian monzogranite extends from 20 to 2008 m below the surface (Lin et al. 2020). We determined the in-situ stress state using core samples retrieved from 1865 to 1959 m in the JM-1 borehole using ASR. Rock mechanics and ASR compliance experiments were conducted to further constrain and evaluate the stress state. Our results can provide a preliminary reference for subsequent geodynamic studies as well as geothermal resources development in the future.

## 2 Geological Setting

The Cathaysia block in southeastern China (Fig. 1A), known for its large exposures of Cenozoic magmatic rocks, is generally believed to have merged with the Yangtze block, stitched along the Shaoxing–Jiangshan–Pingxiang suture zone, and then formed the South China Craton (Zhao and Cawood 2012; Li et al. 2017). Precambrian basement rocks in the Cathaysia area are exposed in the Wuyishan, Chencai, Yunkai, and Hainan regions. The basement rocks are intruded by voluminous granites, diorites, and gabbros

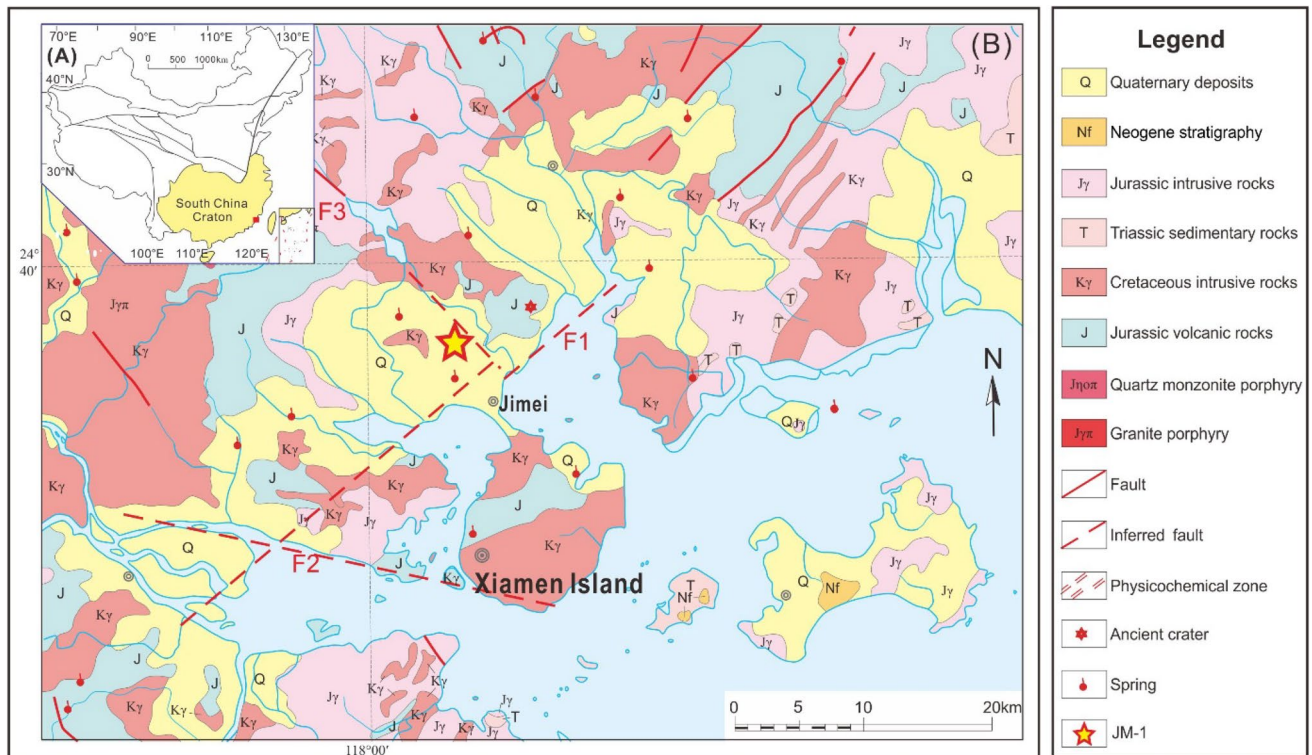


**Fig. 1** **A** Map showing the location of South China. The red rectangle is the study area shown in **(B)**. **B** Map showing the geologic structure and the location of the JM-1 borehole. The fault F1, F2, and F3 are

the CNFZ, Xiamen-Nanjing fault, and Shiweitou-Gaoqi fault, respectively. Note that F2 is a secondary fault of the Jiulongjiang Fault (introduced later)

(Zhou and Li 2000; Shu et al. 2011; Wang et al. 2013) and are overlain by Paleozoic–Mesozoic sedimentary and volcanic rocks (Shu et al. 2014; Li et al. 2014). The Jurassic Yanshanian tectonothermal event created a broad NE-trending fold-and-thrust belt across southern China (Zhou et al. 2006; Yan et al. 2016) associated with the northwestward subduction of the Pacific plate (Zhang et al. 2008; Wang et al. 2013). Subsequent Cretaceous tectonism involved crustal extension that led to widespread basin development and voluminous magmatism (Gilder et al. 1991; Lin et al. 2000; Li et al. 2012). The Cretaceous extension has been interpreted as a back-arc extension induced by slab rollback of the subducting Pacific plate (Li et al. 2014). The extension was punctuated by a compressional episode during the late Early Cretaceous (Wang and Lu 2000; Li et al. 2014), which led to a tectonic inversion of rift basins and produced sinistral and thrust ductile shearing along the coastal Changle-Nan'ao fault zone (CNFZ), geodynamically related to the collision of South China with the Philippine block (Wang and Lu 2000; Wei et al. 2015).

Since the Cenozoic, the Eurasian plate has continuously subducted beneath the Philippine Sea plate (Li et al. 2012). The bedrock along the CRSC is mainly composed of Yanshanian granites and Jurassic and Cretaceous continental facies–volcanic debris. The Cenozoic sediments, such as

the Zhangzhou Basin, Tang'an Plain, and Fuzhou Basin, are mainly Quaternary in age, relatively shallow, and are controlled by the CNFZ and a series of NW striking faults (Fig. 1B). JM-1 borehole is located in the NE striking Mesozoic Zhemin uplift zone bordered by CNFZ and another coastal Binhai fault zone (BFZ). NE-direction CNFZ (F1 in Fig. 1B), EW-direction Xiamen-Nanjing fault (F2), and NW-direction Shiweitou-Gaoqi fault (F3) converge at the mouth of the Jiulongjiang River in the Xiamen Island (Fig. 1B), forming a special geological setting of the JM-1 borehole.

## 3 Methods

### 3.1 Outline of the ASR Method

Natural rock is a viscoelastic material. Accordingly, the stress-induced elastic strain on a rock core recovered from the subsurface is first released instantaneously, followed by a gradual or time-dependent strain release (i.e., anelastic strain recovery). The principle of the ASR method takes advantage of this time-dependent strain release. Voight (1968) first proposed that anelastic strain can be utilized to provide information on in-situ stress states. Matsuki (1991) extended the technique to determine the

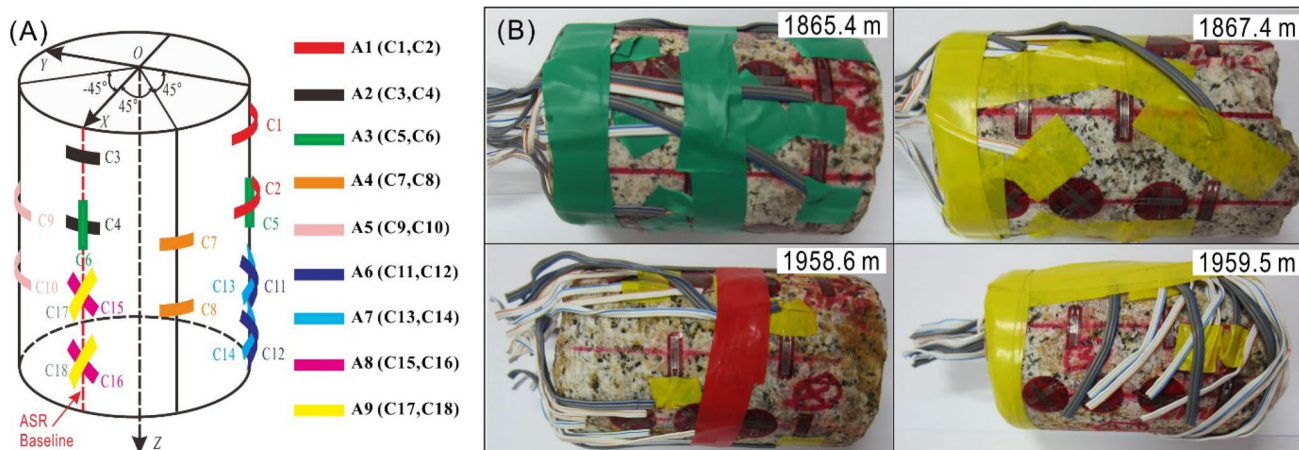


**Fig. 2** **A** Layout of the strain gauges on an ASR core. **B** Four granite cores with gauges glued on the surface from the JM-1 borehole. These pictures were taken after the ASR measurements

three-dimensional stress orientation and showed that it could constrain stress magnitudes. Matsuki (1991) also indicated that, for isotropic viscoelastic materials, the orientations of the three principal in-situ stress components and the three principal anelastic strains agree with each other. Thus, the orientations of the principal in-situ stresses can be determined by calculating the orientations of the principal strains, based on anelastic strain data measured in at least six independent directions.

We express the anelastic normal strain  $\varepsilon_a(t)$  recovered from time 0 to  $t$  in an arbitrary direction with the direction cosines denoted as  $l$ ,  $m$ , and  $n$  with respect to  $X$ -,  $Y$ -, and  $Z$ -axes as (Fig. 2A) (Matsuki 1991; Matsuki and Takeuchi 1993; Lin et al. 2006):

$$\varepsilon_a(t) = \frac{1}{3} [(3l^2 - 1)\sigma_x + (3m^2 - 1)\sigma_y + (3n^2 - 1)\sigma_z + 6lm\tau_{xy} + 6mn\tau_{yz} + 6nl\tau_{zx}] \quad (1)$$

$$Jas(t) + (\sigma_m - p_0)Jav(t) + \alpha_T \Delta T(t)$$

where  $\sigma_x$ ,  $\sigma_y$ ,  $\sigma_z$ ,  $\tau_{xy}$ ,  $\tau_{yz}$  and  $\tau_{zx}$  are the six distinct components of the in-situ stress tensor,  $\sigma_m$  is the mean normal stress,  $p_0$  is pore pressure,  $\alpha_T$  is the linear thermal expansion coefficient,  $\Delta T(t)$  is the temperature variation during the measurement, and  $Jas(t)$  and  $Jav(t)$  refer to the anelastic strain recovery compliance in shear and volumetric deformation mode, respectively. The magnitude of the three-dimensional principal stress can be expressed (Lin et al. 2006):

$$\sigma_i = \frac{e_i(t)}{jas(t)} + \frac{[e_m(t) - \alpha_T \Delta T(t)]}{jav(t)} + p_0 \quad (2)$$

where  $e_i(t)$  ( $i = 1, 2, 3$ ) refers to the anelastic deviator strain and  $e_m(t)$  is the average strain. As can be seen from Eq. (1), the recovered anelastic normal strain of the unloaded rock

$\varepsilon_a(t)$  depends on the in-situ stress components, temperature change during the measurement, thermal expansion coefficient, pore pressure, and compliances of both deformation modes. Therefore, if pore pressure and temperature remain unchanged during the measurement, the stress component can be determined by measuring the anelastic normal strain in at least six independent directions and the anelastic strain recovery compliance of the rock (Fig. 2A). In addition, the orientation of the three principal stresses of an isotropic viscoelastic material is consistent with that of the three principal strains. Thus, the orientations of the three-dimensional principal in-situ stresses can be determined by calculating the principal strain orientations (Matsuki and Takeuchi 1993; Lin et al. 2006).

Compared with other core-based and borehole-based methods, the ASR method is considered to be a low-cost and high-efficiency technique (Wolter and Berckhemer 1989; Sun et al. 2017; Wang et al. 2020). Strain measurements are often conducted on site as soon as rock cores are retrieved from boreholes. In this regard, the ASR method can be deemed a quasi-in-situ stress measurement method. However, the ASR method is subject to some limiting factors, such as temperature variation, core dehydration, rock anisotropy, insufficient strain recovery time and the accuracy of core orientation (Zang and Stephansson 2010). Like most core-based techniques, reliable estimation of in-situ stress tensors from anisotropic cores has not yet been properly addressed.

### 3.2 Rock Sampling and the ASR Measurement Procedures

Four high-quality granite core samples (~11 cm in length and ~68 mm in diameter) were collected from the JM-1 borehole. Two cores were retrieved from ~1870 m in depth and



two were from ~1960 m in depth (Fig. 2B). All the samples are smooth-surface cylindrical cores and composed of medium–coarse-grained granites of Cretaceous age (Lin et al. 2020). We conducted ASR measurements and analyses, adopting the guidelines and suggested apparatus of Lin et al. (2007) and Byrne et al. (2009), respectively. After the samples were removed from the coring bit, they were immediately washed and air-dried at room temperature, then marked with baselines at 45° to ensure that strain was measured in at least nine directions, six of which were independent. A total of eighteen strain gauges, providing double redundancy and mutual calibration were glued to the core surface as deployed in Fig. 2A and connected to a strain acquisition system that collected data every 20 s for 5.5–7.0 days. The prepared samples were double wrapped in plastic and aluminum bags, both of which were sealed with silicone rubber to avoid pore-water volatilization during the measurements. The wrapped samples were submerged in a thermostatic water tank, where temperature changes were controlled to within  $\pm 0.5$  °C. Meanwhile, a dummy granite specimen that does not undergo any deformation was prepared in the same manner and placed in the same tank to monitor data drift of the acquisition system (Lin et al. 2006). Generally, anelastic strain recovers continuously over several days or weeks after the initial stress release, but the recovery rate decreases steeply over time. Hence, field ASR measurements should start as soon as possible. We selected deeper cores from the coring operation to shorten the time interval from the initial stress release due to drilling to the start of the ASR measurements. All the time intervals in our measurements were less than 8 h. Although the JM-1 borehole is located in a geothermal area, the temperature at the bottom of the hole is still below 70 °C. After a certain period (~5 h) of scouring and soaking in the circulating fluid in the drill pipe, the core has been sufficiently cooled when it reaches the ground surface. Furthermore, before the ASR data collection, the temperature of the core surface has been the same as that of the circulating water in the tank, reaching a state of thermal equilibrium. Therefore, the thermal stress on the surface of the ASR core can be reasonably ignored.

After the ASR measurements, paleomagnetic analyses were conducted to restore the directions of the principal stress axes to their original geographic coordinates (see Yamamoto et al. 2013). The ASR core can be oriented by comparing the direction of the viscous remnant magnetic (VRM) component in the geographic coordinate system with that of the contemporary geomagnetic field. Then, the baseline orientations (Fig. 2A) on the cores were reoriented to the geographic reference frame by VRM analyses using sub-samples from the ASR cores. The VRM of 3–7 sub-samples from each ASR core were measured using the principal vector method (Wang et al. 2020) with a superconducting

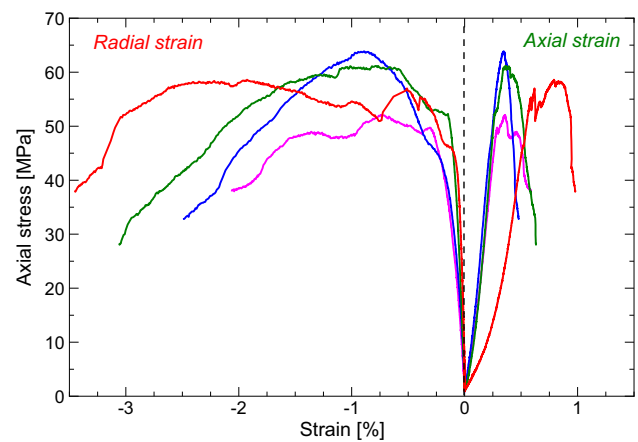


**Fig. 3** Axial and radial strain curves with key deformation characteristics. Four pairs of strain curves with different colors denote four granite sub-samples from ~1865 and ~1959 m in depths, where contractional strains are defined as positive. Note that peak strength values of samples from the JM-1 borehole are relatively lower than common granites, which generally have a UCS value larger than 100 MPa

magnetometer (2G-755R, USA) at the Institute of Geomechanics, Chinese Academy of Geological Sciences.

### 3.3 Rock Mechanics and ASR Compliance

In traditional ASR measurement procedures, for simplicity, the key parameter for the principal stress calculation, the ratio of the two ASR compliances (see its definition later), is usually assumed to be constant (Lin et al. 2006). In this study, the ASR compliance was calibrated in the laboratory to ensure and improve the accuracy of 3D principal stress. Before calibrating the ASR compliance, it is necessary to conduct rock mechanics experiments to obtain the uniaxial compressive strength of the ASR cores. The purpose is to provide the pressure reference value for the ASR compliance calibration. In addition, the basic mechanical characteristics of the granite from the JM-1 borehole can be understood. Rock mechanics experiments were conducted to evaluate the characteristics of the ASR cores using sub-samples from the two sampling depths (~1865 and ~1959 m). Sub-samples were drilled approximately coaxially from some ~68 mm diameter cores. A total of 12 cylindrical sub-samples of 1 inch in diameter and 2 inches in height were made in the laboratory. With the same depth and lithology, these sub-samples allow better evaluation of the mechanical properties of cores subjected to ASR stress measurements.

Uniaxial compression tests were conducted to directly measure the strength and deformation properties of the granites. Experiments were conducted using axial strain rates of  $10^{-5}$  s<sup>-1</sup> until sample failure occurred. The typical stress–strain curves of the samples are shown in Fig. 3. The non-linear concave phases at the beginning of deviatoric

loading may be related to the gradual closure of pre-existing microcracks. After the initial increase, a quasi-linear stress–strain phase is obtained that represents the elastic behavior of the granite. From the peak stress and in the post-peak regime, microcracks coalesce and macroscopic cracks occur (Horii and Nemat-Nasser 1985; Eberhardt et al. 1998). To characterize the elastic behavior of the granites under unconfined compression tests, we used the linear part of the loading stress–strain curve, which approximately corresponds to 40 and 60% of the peak compression strength, respectively, to calculate the elastic modulus and Poisson's ratio (Yin et al. 2016). The mean and standard deviation of unconfined compressive strengths (UCS) for the four sub-samples was  $57.0 \pm 5.1$  MPa, indicating that the mechanical strength of the shallow crustal granites is relatively weak. The grain size of granite cores from the JM-1 borehole was medium-coarse scale. Also, significant millimeter-scale and visible microcracks were found on the surface of the ASR cores. Eberhardt et al. (1999) stated that the strength of brittle crystalline rock tends to decrease with increasing grain size because of the coalescence effect related to longer grain boundaries and larger intergranular cracks. However, further investigation and studies are necessary to clarify this issue.

Further extension to 3D stress magnitudes requires the assumption that the rock is an isotropic and linearly viscoelastic material with two independent modes of shear and volumetric deformation (Matsuki 1991; Byrne et al. 2009). By applying the correspondence principle of linear viscoelasticity and making the assumption that the bulk modulus of the rock matrix is not a viscoelastic parameter, Matsuki (1991) reported that the recovered anelastic normal strain depends on the in-situ stress tensor, pore pressure, and the compliances of both deformation modes. A term called ASR compliance ratio is defined as the ratio of the shear and volumetric deformation modes (i.e.,  $Jas(t)/Jav(t)$ ) and is needed to convert from the anelastic strain to the principal stress. However, previous studies (e.g., Matsuki and Takeuchi 1993; Lin et al. 2006; Matsuki 2008) have shown that this ratio exhibits a lithology-dependent feature and has been usually assumed to be a constant (commonly 2 for granites). However, unlike high strength and somewhat rigid typical granite, the rock mechanics tests in this study yielded unusually weak strengths of the granite samples in the JM-1 borehole, indicating that laboratory measurements of ASR compliance, rather than an assumed value, are therefore necessary to estimate the in-situ stress more accurately (e.g., Matsuki 2008; Gao et al. 2014). We prepared a sub-core for these ASR compliance measurements in the laboratory. Two cross-gauges were glued to the cylindrical surface at  $90^\circ$ . A syringe pump was used to load the sub-core specimen. Because core recovery from great depths often takes more than a few hours (even  $> 10$  h), a

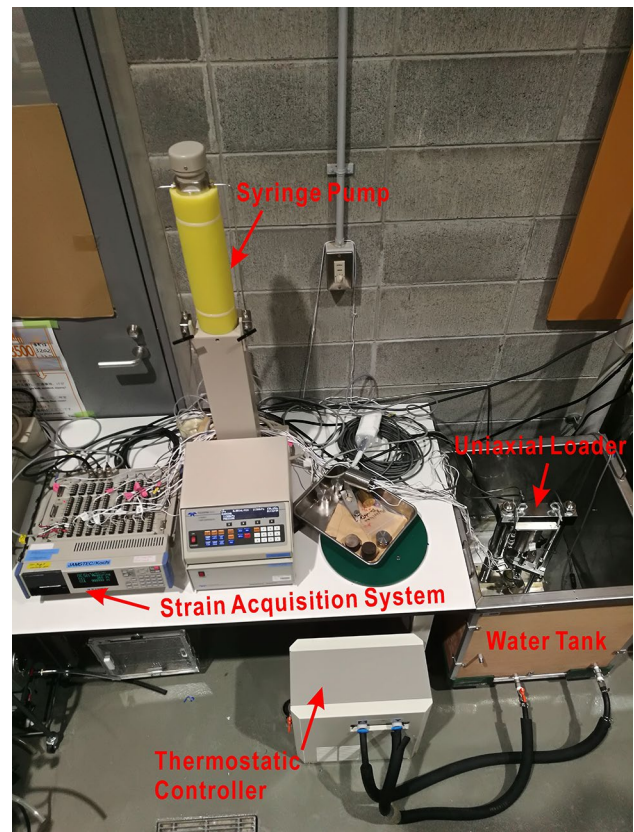


**Fig. 4** The ASR compliance measurement of granite sub-sample in a laboratory of Kyoto University. The strain acquisition system was the same type as ASR stress measurements in the JM-1 borehole field. Uniaxial pressure acting on the sub-core was transmitted by high-pressure freshwater from the syringe pump. Room temperature was fluctuating from 23.3 to 26.0 °C during the experiment. However, the water temperature in the tank was kept constant at  $25 \pm 0.5$  °C by the water circulation of the thermostatic controller

long-term ASR compliance measurement for better in-situ stress estimation is recommended by Matsuki (2008) and Gao et al. (2014). Here, we pre-loaded the specimen at a constant pressure of  $\sim 50\%$  of the UCS for 48 h to perform creep tests, then reduced the pressure instantaneously to zero while collecting ASR measurements that continued for 9 days (Fig. 4). A dummy core was also used throughout the test.

Due to the presence of microcracks caused by stress or cooling during core recovery, both the elastic strain and anelastic strain are affected to some extent. Only one group of ASR compliances (i.e.  $Jas(t)/Jav(t)$  ratios) show the expected anelastic and time-dependent curve (see fig. 1 in Matsuki (2008) and hereafter Fig. 5). Therefore, this  $Jas(t)/Jav(t)$  ratio was suitable for stress estimation. Overall, both the shear and volumetric modes increased over time, but the rate of increase decreased after approximately 1.5 days. Previous studies (e.g., Matsuki 2008; Gao et al. 2014) have shown that the long-term  $Jas(t)/$

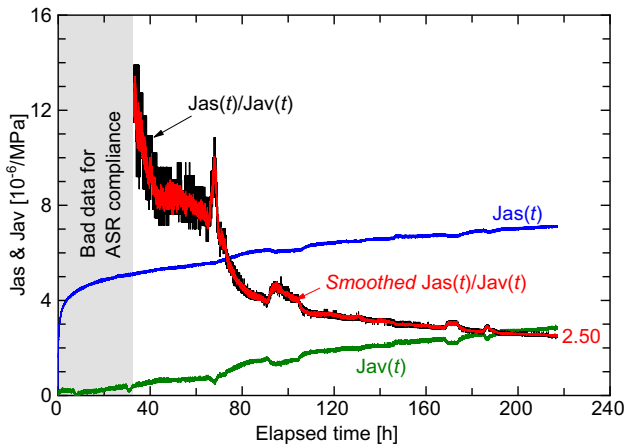


**Fig. 5** Time profiles of shear and volumetric mode compliances, as well as the  $Jas(t)/Jav(t)$  ratio for the sub-core from the JM-1 borehole after the release of the uniaxial compressive pre-loading at ~50% of the UCS. In the first 33 h after pre-loading, the increase in  $Jav(t)$  was so small that very small changes produced drastic fluctuations in the  $Jas(t)/Jav(t)$  ratio, which is not suitable for ASR compliance calculations. The blue and green curves corresponding to  $Jas(t)$  and  $Jav(t)$  donate shear and volumetric deformation with time, respectively. The black curve donates  $Jas(t)/Jav(t)$  ratio of ASR compliance. The red curve represents the smoothed result of the  $Jas(t)/Jav(t)$  ratio and reaches a final value of 2.50, gradually. Note that there are three raised steps after the 80 h due to temperature disturbance by adding water into the tank

$Jav(t)$  ratio remained essentially unchanged for 10 h. However, our measurements show that, except for the drastic fluctuations in the first 33 h, the  $Jas(t)/Jav(t)$  ratio decreased rapidly from ~12 to ~4 within the following 50 h, then slowly decreased to 2.5 over the next 5.6 days (Fig. 5). It seems that this rapid decline in the  $Jas(t)/$

$Jav(t)$  ratio at the beginning of the test may be due to the presence and opening of microcracks. Nevertheless, the extent to which microcracks will affect the compliance of ASR cores requires further investigations in the future.

## 4 Results

### 4.1 Anelastic Strain Recovery

The anelastic strain values of granite cores recovered during 5.5–7.0 days in various directions ranged in ~15–200 microstrains (Fig. 6), which are sufficiently high relative to the measurement accuracy of the system such that the data can be used for 3D stress analysis. Based on the measured anelastic normal strain values, the anelastic strain tensors were calculated as a function of time ( $t$ ) using a least squares analysis. The calculated results include the principal strain components  $\epsilon_{1,2,3}(t)$  and the mean normal strain  $\epsilon_m(t)$  (Fig. 6). It is reasonable to consider the granite cores as homogeneous and isotropic materials, such that the orientations of the principal anelastic strain and the principal in-situ stress can be assumed to be the same (Matsuki 1991), thus obtaining 3D in-situ stress orientations (Fig. 7) and ratios of the principal stress deviations.

### 4.2 Magnitudes of In-Situ Stresses

As mentioned earlier, the ASR method can obtain three-dimensional stress states, namely  $\sigma_1$ ,  $\sigma_2$ , and  $\sigma_3$ , which reveal the true crustal stress state under the background of tectonic movement. The free surface of the Earth is in contact with air or water is also a principal stress plane since it cannot

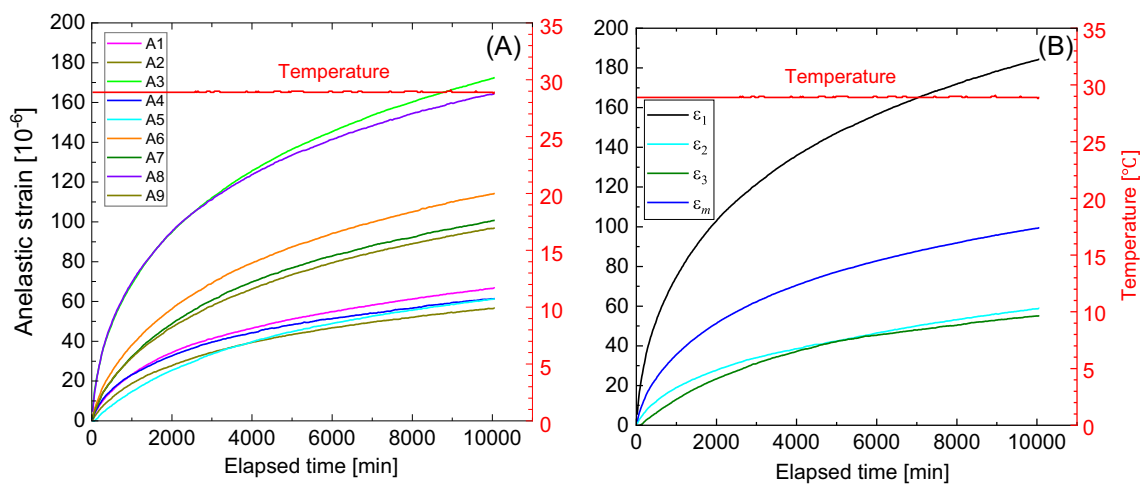


**Fig. 6 a** Anelastic normal strain recovery curves for the core specimen from 1959.5 m, where extensional strains are defined as positive. The labels A1–A9 in the box show the measurement directions of the normal anelastic strain shown in Fig. 2A. The water temperature was

held at  $29.0 \pm 0.5$  °C throughout the measurements. **b** Three principal anelastic strain values  $\epsilon_{1,2,3}$  and mean constant strain  $\epsilon_m$  as a function of time. See the unit of temperature on the right axis label

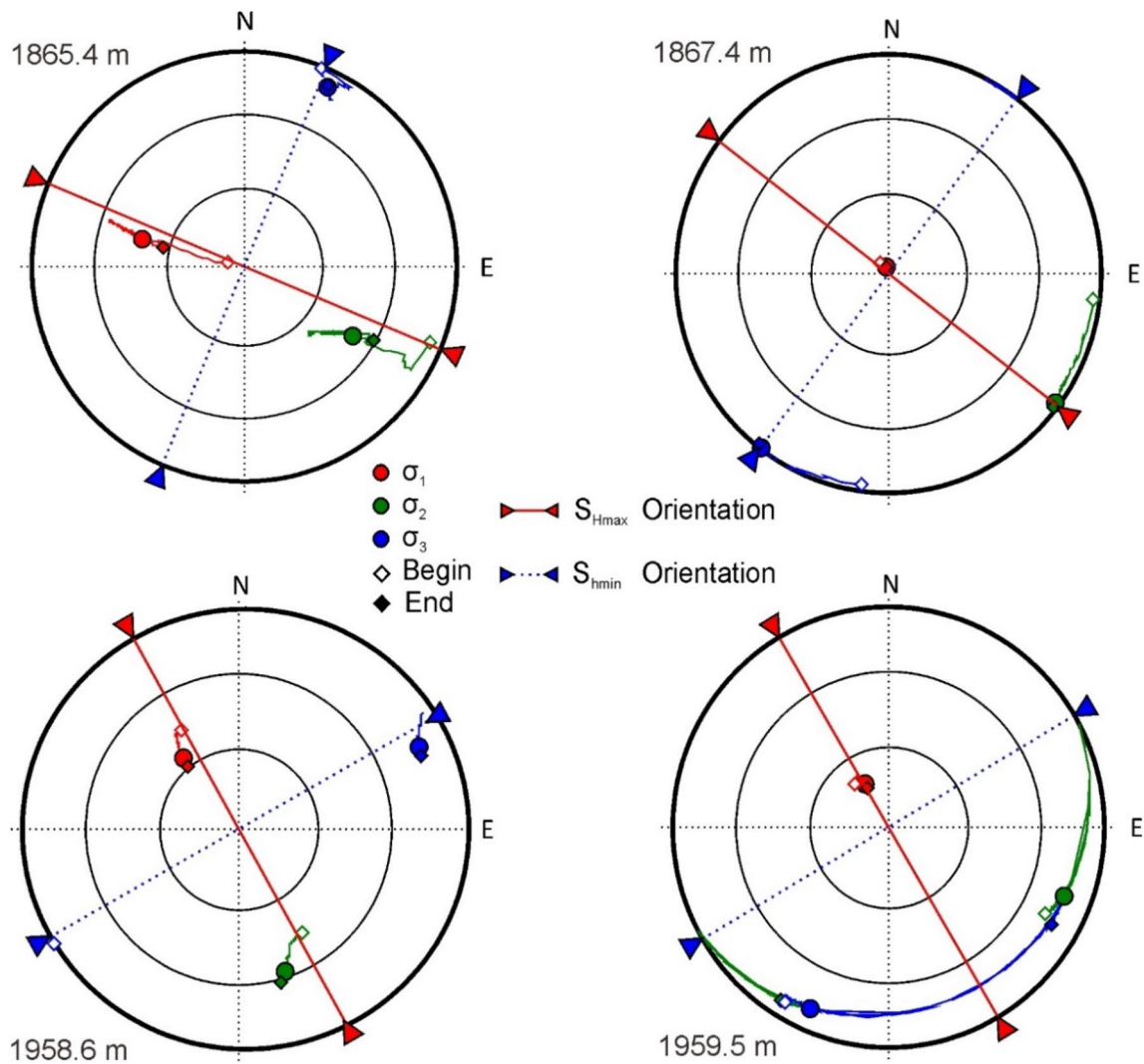


**Fig. 7** Orientations were determined for three-dimensional principal in-situ stresses in four samples from the JM-1 borehole. Open diamond symbols represent the orientation at the beginning of the ASR test and solid diamonds represent the orientation at the end of the test; the solid circles present average orientation from the anelastic

strains except at an early stage of the ASR test (Refer to text). Note that  $\sigma_2$  and  $\sigma_3$  changed widely during the measurement for the core specimen from 1959.5 m, which is consistent with changes in the principal anelastic strain  $\varepsilon_2$  and  $\varepsilon_3$  shown in Fig. 6B

sustain shear force (Zoback 2007). Thus, one principal stress, generally assumed as the vertical stress,  $S_v$ , is normal to the Earth's surface, while the other two principal stresses, named  $S_{Hmax}$  and  $S_{Hmin}$ , act in an approximately horizontal plane. It is verified that it is generally true from the earth's surface to the depth of the brittle-ductile transition in the upper crust at ~15–20 km depth, according to the compilation of earthquake focal mechanism data and other stress indicators (Zoback 1992). In this study, both types of principal stress are listed in Table 1. However, for clear analysis and discussion, the magnitudes and orientations of the vertical and horizontal principal stresses will be more involved in the following text.

We used the measured long-term  $Jas(t)/Jav(t)$  ratio of 2.50 to obtain the three-dimensional principal stress magnitudes (Fig. 5). The horizontal principal stresses ( $S_{Hmax}$  and  $S_{Hmin}$ ) are not directly measured but are obtained by resolving the 3D principal stresses on the horizontal plane according to their trends and plunges. We assumed that the vertical stress ( $S_v$ ) was equal to the density-related overburden stress from surface to 1959.5 m. The density of granite was measured in the laboratory using cores of different depths in the JM-1 borehole, and the average value is  $2.64 \text{ g/cm}^3$ . The pore pressure ( $p_0$ ) was calculated using the water density, assuming hydrostatic pressure (Yamamoto et al. 2013). The groundwater level of the JM-1 borehole is ~200 m below the ground



**Table 1** Orientations and magnitudes of the in-situ stresses of the ASR measurement

No	Depth (m)	Orientations (°)						Magnitudes (MPa)						$S_{Hmax}$ Ori. (°)
		$\sigma_1$		$\sigma_2$		$\sigma_3$		$\sigma_1$	$\sigma_2$	$\sigma_3$	$S_{Hmax}$	$S_{hmin}$	$S_v$	
		Tr	Pl	Tr	Pl	Tr	Pl							
1	1865.4	285.0	48.8	122.5	39.8	25.1	8.7	53.3	45.0	34.7	48.7	35.0	49.3	N67°W
2	1867.4	336.8	87.4	129.8	2.3	219.9	1.2	49.3	36.1	34.0	36.1	34.0	49.3	N50°W
3	1958.6	322.9	56.1	162.9	32.2	67.0	9.3	55.8	43.8	37.4	47.6	37.7	51.7	N28°W
4	1959.5	334.5	72.3	113.7	13.6	206.4	11.1	53.2	38.9	38.3	40.1	38.5	51.7	N27°W

Tr trend, Pl denotes plunge

surface and hydrostatic pressure was adopted to calculate the principal stress magnitudes in this study.

In Table 1, the results show that from ~1865 and ~1959 m in depth,  $\sigma_1$  is approximately 49.3–55.8 MPa, whereas  $\sigma_2$  and  $\sigma_3$  are 36.1–45.0 MPa and 34.0–38.3 MPa, respectively. The relationship between the three principal stresses and  $S_v$  is relatively clear:  $\sigma_1 > S_v > \sigma_2 > \sigma_3$ . In addition, the maximum and the minimum horizontal principal stresses are 36.1–48.7 and 34.0–38.5 MPa, respectively. The vertical principal stresses are 49.3–51.7 MPa. According to Anderson's faulting theory, the three-dimensional principal stresses are characterized by  $S_v > S_{Hmax} > S_{hmin}$ , indicating that the effects of gravitation on the regional stress field is stronger than that of the tectonic plate motion. Furthermore, the normal-faulting stress regime indicated by the data implies the presence of an extensional environment in this region. Lin et al. (2006) showed that a common range of  $Jas(t)/Jav(t)$  ratio from one to three would have a relatively small influence on the magnitudes of the principal stresses. Furthermore, the relationship between the three principal stress values (the stress regime) remains unchanged regardless of the different  $Jas(t)/Jav(t)$  ratios. The change law of the three principal stresses is characterized by linear formulas, as shown in Fig. 8. Due to the lack of data constraints above 1865 m in the borehole, we assumed that the principal stresses at the surface are zero.

### 4.3 Orientations of In-Situ Stresses

Few published studies have used paleomagnetic analyses to restore the geographic coordinates of granite samples. Here, we obtained principal stress orientations by redirecting the core baseline relative to the geographic north. Among them, the two cores that are close to each other exhibit relatively consistent principal stress directions, respectively (see Fig. 7). The principal stress orientations measured must be unique for a certain core sample. However, the orientations calculated by anelastic strain at an arbitrary time from measurement beginning varies with time due to anelastic strain measurement accuracy. At an early stage of the whole measurement period, the calculated orientations of the principal strains scatter significantly because the ratios

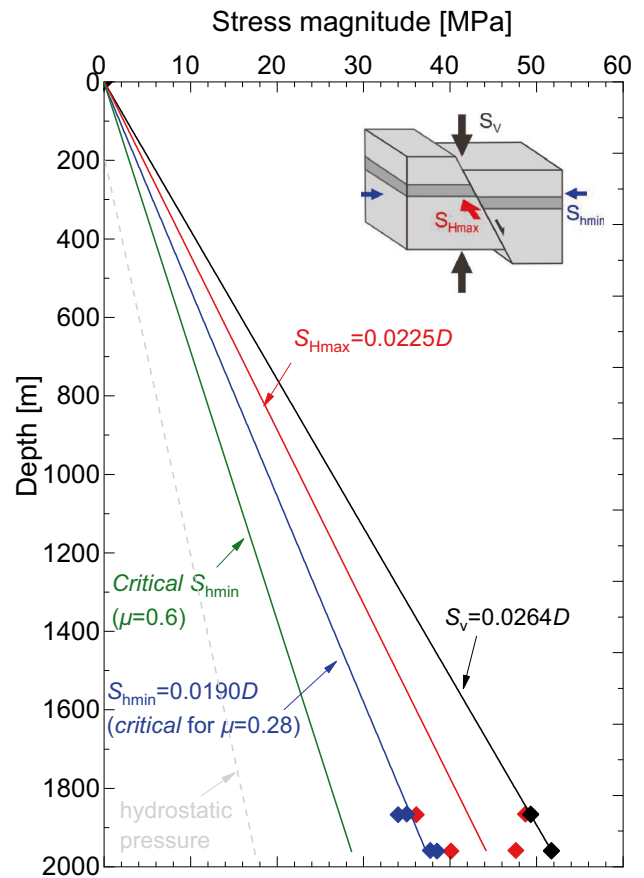


**Fig. 8** Horizontal and vertical principal stress magnitude profiles for the JM-1 borehole. The parameter  $D$  of linear formulas represents the borehole depth. The results indicate a normal-faulting stress regime, illustrated by the cartoon in the upper right corner. A critical  $S_{hmin}$  ( $\mu=0.6$ ) is also shown according to the Mohr–Coulomb frictional-failure criterion

of the deviations of principal anelastic strains are unstable when the maximum component of principal strain deviation (Eq. 2), was small. Consequently, we averaged the time data series of the three principal strain orientations, respectively, using data that excluded the first 200 min of the early stage.

For the sample from 1865.4 m, the plunge of  $\sigma_1$  is 48.8°, which is not consistent with the vertical stress  $S_v$ . The other

three samples all have a sub-vertical maximum principal stress ( $\sigma_1$ ) with a plunge  $56.1^\circ$ – $87.4^\circ$ , while the intermediate ( $\sigma_2$ ) and minimum ( $\sigma_3$ ) principal stresses are sub-horizontal (Table 1). For the normal faulting stress regime,  $\sigma_1$  and  $\sigma_2$  correspond to  $S_v$  and  $S_{Hmax}$ , respectively. The trends of  $\sigma_2$  are  $113.7^\circ$ – $162.9^\circ$ , which are close to the  $P$ -axis directions of the focal mechanism solutions in the Xiamen region (Hu et al. 2017), stating the test reliability of paleomagnetic orientation. On the other hand, the maximum horizontal principal stresses ( $S_{Hmax}$ ) are oriented at  $N67^\circ W$ ,  $N50^\circ W$ ,  $N28^\circ W$ , and  $N27^\circ W$ , from 1865.4 to 1959.5 m, respectively. Except for 1959.5 m, the orientations between  $S_{Hmax}$  and  $\sigma_2$  have good consistency (Table 1). Moreover, the  $S_{Hmax}$  directions of the two samples with similar depths agree with each other very well. Overall, the averaged  $S_{Hmax}$  direction of all samples is  $N43^\circ \pm 19^\circ W$ , which agrees with previous findings (Gao et al. 2009; Lin et al. 2009; Zhang et al. 2013) and is generally consistent with the subduction direction of the Philippine Sea plate towards the Eurasian plate.

#### 4.4 Analysis of Regional Faults Activity

Byerlee (1978) compiled an extensive dataset of laboratory friction measurements derived from natural joints in rocks, failure discontinuities in triaxial compression tests and artificial joints with various roughness, concluding that friction is nearly independent of the rock type and deriving the frictional coefficient,  $\mu$ , of 0.6–1.0, commonly known as Byerlee's law. The strength of a critically stressed fault can be estimated by evaluating the limited frictional coefficient. Stress states obtained from in-situ measurements in the upper crust agree well with the failure equilibrium (Townend and Zoback 2000). The ratio of maximum effective principal stress to minimum effective principal stress, which corresponds to the case in which critically stressed faults and fractures are at the frictional limit is given by Jaeger and Cook (1979) as

$$\frac{\sigma_1 - P_0}{\sigma_3 - P_0} = \left( \sqrt{1 + \mu^2} + \mu \right)^2 \quad (3)$$

where  $\mu$  is the frictional coefficient of faults or preexisting fractures.

According to Anderson's faulting theory (Anderson 1951), Eq. (3) should take a different form for a normal-faulting stress regime

$$\frac{S_v - P_0}{S_{hmin} - P_0} \geq \left( \sqrt{1 + \mu^2} + \mu \right)^2 \quad (4)$$

If crustal stress reaches the frictional strength of critically stressed faults and fractures, frictional sliding will occur along the optimally orientated planes, which can be given by

$$\beta = \frac{1}{2} \left( \frac{\pi}{2} + \tan^{-1} \mu \right) \quad (5)$$

where  $\beta$  is the angle between the normal of a fault or fracture plane and the direction of the maximum horizontal principal stress.

In an area of critically stressed normal faults, when pore pressure is hydrostatic and  $\mu = 0.6$ , the lower bound value of the minimum principal stress  $S_{hmin}$  is  $\sim 0.6 S_v$  (Zoback 2007). From Fig. 8 we can see that, no  $S_{hmin}$  value approaches the lower bound (commonly  $\mu = 0.6$ ) determined by the Coulomb frictional-failure criterion and Byerlee's law. However, clay and other minerals contained in the natural faults, such as montmorillonite or vermiculite, will reduce the frictional coefficient, and therefore reduce the frictional strength consequently (Byerlee 1978). Some researchers reported that the frictional coefficient will be lower in an actual fault than predicted (Zoback 2007; Colletini et al. 2019). Carpenter et al. (2011) found that natural serpentines near the San Andreas Fault system at depth exhibited low frictional coefficients (only 0.18–0.26). Here, it was inferred that the stress state in the deep of the JM-1 borehole could be critical normal-faulting if the frictional coefficient of optimal-orientated faults is close to 0.28 (Fig. 8).

## 5 Discussions

### 5.1 Validity and Reliability of Stress Measurement Data of JM-1 Borehole

Generally, integrating stress data from multiple measured methods can help better constrain and improve the reliability of in-situ stress results in a borehole or an area (Zang and Berckhemer 1993; Ask et al. 2009). For deep boreholes, hydraulic fracturing is often considered to provide high-quality complementary in-situ stress data, especially the  $S_{hmin}$  values. Unfortunately, there is no available hydraulic fracturing test data from the depth of 2 km of the JM-1 borehole. By careful examination of a section of the ultrasonic imaging log, slight borehole breakouts or spallings were confirmed, which can be used to indicate the principal stress directions. It is well known that in vertical wells, borehole breakouts are the enlargement of a wellbore wall at the azimuth of the  $S_{hmin}$  resulting from rock failure or grains fall-out under significant excess differential stress (Zoback 2007). As shown in Fig. 9, a discontinuous but identifiable borehole breakout image from a depth of  $\sim 1871.0$  to  $\sim 1874.5$  m manifests that the direction of the  $S_{hmin}$  is  $N38^\circ \pm 24^\circ E$  and thus the direction of the  $S_{Hmax}$  is  $N52^\circ \pm 24^\circ W$ . This agrees well with the results of the  $S_{Hmax}$  directions determined by the paleomagnetism of the ASR cores at  $\sim 1865$  and  $\sim 1867$  m

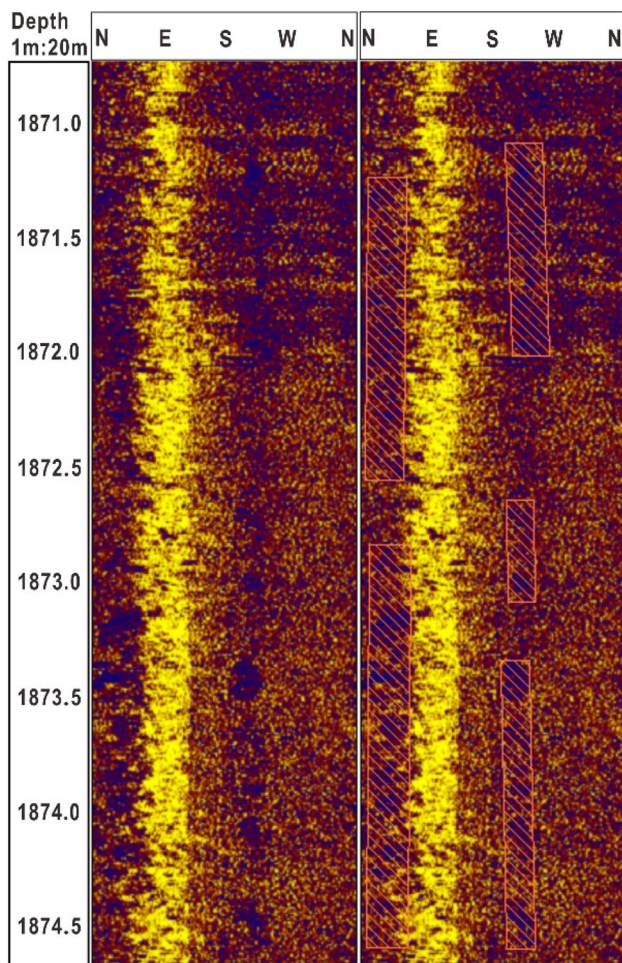


**Fig. 9** Borehole breakout or spalling image revealed by ultrasonic borehole image logging from ~1871.0 to ~1874.5 m section of the JM-1 borehole

(Table 1), indicating the reliability of the principal stress directions of the ASR cores determined in this study.

As mentioned previously, all core-dependent stress measurement methods are based on the assumption that the rock is a homogeneous and isotropic material (Zang and Stephansson, 2010). According to extensive investigations and literature, it is reasonable to consider granite as a homogeneous and isotropic material, regardless of its grain size. Overall, it is a valid and acceptable assumption for the ASR cores in this study. Zang and Berckhemer (1993) examined anelastic strain recovery and ultrasonic wave velocity of core samples in the KTB pilot hole and quantified the alterations of physical properties of crystalline rock caused by time-dependent, stress-relief microcracking within the recovered cores, which revealed the possible influencing factors of ASR in-situ stress measurements of large-depth boreholes. Further investigations showed that crack-induced anisotropy played an important role in total rock anisotropy (Zang et al. 1996).

Teufel (1983) assumed the nature of the anelastic strain recovery process to be a consequence of crack formation and stated that the initially measured strains are more significant than those at the end of the recovery process for the stress estimation of the directions and magnitudes. Our ASR cores started strain acquisition in less than 8 h after cut from the borehole bottom. The anelastic strain values of granite cores of the JM-1 borehole were ranged in ~15–200 microstrains, which are well consistent with those of ASR cores of the KTB pilot hole taken from a depth of 1488–3858 m (Zang and Berckhemer 1993). There were some visible millimeter-scale microcracks on the surface of the ASR cores of the JM-1 borehole. However, whether these microcracks are mainly parallelly oriented and to what extent they may affect the results of in-situ stress measurements are not yet well understood and require further study. It is worth noting that the comparative measurements of ASR and another core-based stress test method, that is, differential strain curve analysis, have been performed in Hijiori hot dry rock boreholes in Japan, and the results show that the ASR measurement data are helpful and reliable (Oikawa and Yamaguchi 2000). The magnitudes and directions of principal stresses obtained by these two methods were similar to each other, which was verified by the microseismic clusters characteristics of hydraulic fracturing conducted later (Tezuka and Niitsuma 2000).

## 5.2 Stress Characterize in the CRSC

Converging plates increase horizontal compression. Frontal collisions of large plates at relatively high velocities usually imply high tectonic stress accumulation rates associated with strong earthquakes near the plate margins. However, our measured stress results seem to indicate that it is not the case in the CRSC. As can be seen from Fig. 8, the horizontal stress difference only increases by 3.50 MPa/km and the  $S_{Hmax}$  magnitude is equal to 0.85 Sv, indicating a relatively low-stress accumulation in the shallower range of <2 km (in the shallow crust) in the Xiamen region. As mentioned earlier, the strength of the Yanshanian granite in the JM-1 borehole is quite weak. Nonetheless, imaging logs showed few borehole breakouts, or only mild spallings on the borehole wall (Fig. 9), further indicating that the differential stress in this region is relatively small. In this study, in-situ stress measurements in the JM-1 borehole show that the shallow crust in the Xiamen region of the CRSC is mainly controlled by the vertical stress due to gravity, indicating an extensional stress field. This probably reflects the influence of the nearby NW striking Jiulongjiang fault zone that formed during the Mesozoic and is still active, with normal and sinistral strike-slip faulting patterns (Ma 1989). The horizontal stress difference or shear stress level is relatively low, which indicates that the compression between the Eurasian



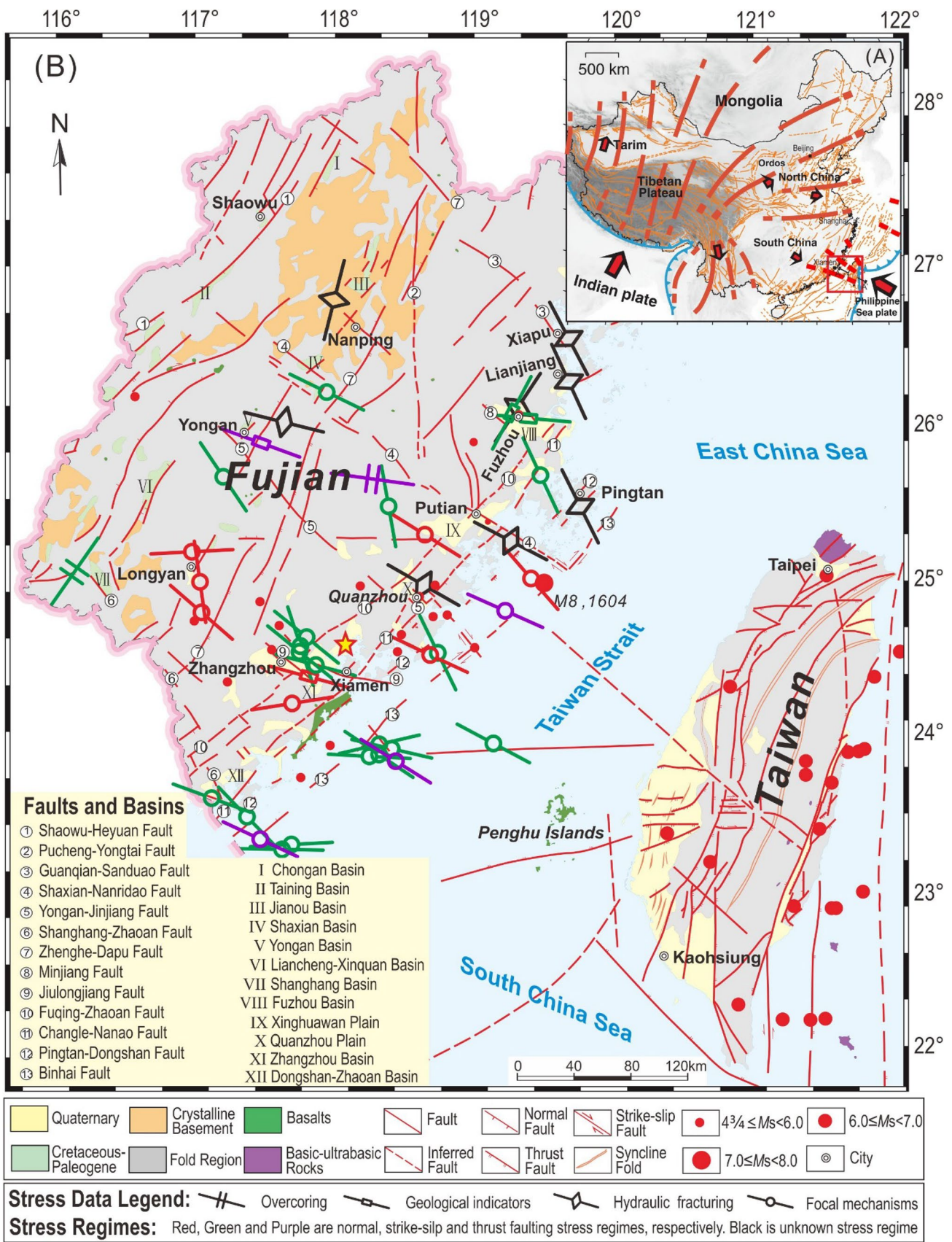




**Fig. 10** **A**  $S_{Hmax}$  stress trajectory and tectonic environment of China and the adjacent regions (modified from Liu et al. (2011) and Hu et al. (2017)). The JM-1 borehole is located in Xiamen city and is controlled by a fan-shaped local stress field resulting from the north-westward movement of the Philippine Sea plate. **B** Simplified present geologic setting and active faults in the CRSC and Taiwan (modified from Ma et al. 1989). Stress data are collected from Xie (2015), Zhang et al. (2015), Li et al. (2016), and some unpublished hydraulic fracturing stress results. The star represents the JM-1 borehole. Note that only stress data in the CRSC are collected and shown here

plate and the Philippine Sea plate is weak at shallow depths. Xu et al. (1999) analyzed borehole breakout data from offshore oil wells adjacent to the northern Taiwan Strait and concluded that the shear stress was relatively small. Some hydraulic fracturing in-situ stress measurements were conducted above 500 m depth in coastal areas in need of rock engineering construction (Zhang et al. 2015; Li et al. 2016). All of these borehole stress magnitudes indicated low stress levels. Furthermore, stress regimes were characterized by strike-slip and normal faulting and may be affected by NW and NE trending faults in the coastal region from Xiamen to Fuzhou, except for Quanzhou, which is located in the middle. A destructive earthquake with a magnitude of ~8 occurred offshore of Quanzhou in 1604, which was also the largest earthquake in the historical record in the CRSC (Zhang et al. 2018), implying that the tectonic environment in Quanzhou is prone to accumulating stress and developing strong earthquakes (Fig. 10B). Hydraulic fracturing results from Quanzhou indicate a thrust faulting stress regime and high compressive stress accumulations (Zhang et al. 2015), coinciding with its seismicity conditions.

In the hydraulic fracturing in-situ stress measurements of previous studies, a routine operation named impression testing was conducted to obtain information on the  $S_{Hmax}$  directions. For the northern coast of the CRSC, impression tests showed that the average orientation of the  $S_{Hmax}$  is N33°W in Fuzhou and Xiapu (Li et al. 2016). In the middle part of the coast, the  $S_{Hmax}$  orientations are N54°W and N52°W in Quanzhou (Zhang et al. 2015) and Xiamen, respectively. The CRSC is seismically active, we collected available stress indicators from the focal mechanism (Fig. 10B). The stress directions from the focal mechanism are close to and sub-parallel to several major NW striking active faults (Fig. 10B), which seems to be consistent with the tectonic feature of the study area dominated by strike-slip active faults. It should be pointed out that the measured stress directions by the hydraulic fracturing method are similar to those by the focal mechanism method, indicating that the regional principal stress directions may be consistent from shallow to deep. Understanding the stress orientation at a local scale, the plate boundary forces, especially the convergence and compression of the Eurasian and Philippine Sea plates, play a first-order role in controlling the crustal stress

patterns. To some extent, the influence of the northward collision of the Indian plate cannot be ignored. However, it is hard to evaluate and understand its role clearly and intuitively based on the results of this study.

The newly integrated China Stress Database shows that there are two opposing fan-shaped stress patterns in eastern China (Hu et al. 2017). On a continental scale, the  $S_{Hmax}$  orientations rotate clockwise from the north to the south along the coastal line and towards the sea (see fig. 4 in Hu et al. (2017) in detail). In contrast, regional-scale  $S_{Hmax}$  orientations rotate counterclockwise from the north to the south, disturbing the clockwise rotation in the CRSC and causing the local stress heterogeneity (Fig. 10A). Some researchers have interpreted this as a consequence of the tectonic knot effect (Hu et al. 2017) or the indenter model (Ranjbar-Karami et al. 2019) of the compressing block. Therefore, we can further conclude that the interaction of the two plates generates a regional crustal stress field in the CRSC and the Philippine Sea plate seems to play a more important role in controlling or enhancing the inhomogeneity of the local stress pattern.

### 5.3 Regional Active Tectonics Related to Stress Field of CRSC

The CRSC is considered tectonically active and is mainly divided and controlled by two sets of active faults that strike NE and NW, as shown in Fig. 10B. The NE–NEE striking Binhai fault zone (BFZ) is a strike-slip lithospheric fault that developed along the coastal zone and is ~400 km in length and ~12 km in width (Xu et al. 2006). It is also believed to be the boundary fault between South China and the South China Sea Blocks. The crustal structure on the NW side of the BFZ is ~30 km thick normal continental crust, while the SE side is thinning continental crust with a thickness of 25–28 km (Huang et al. 2014). The left-lateral strike-slip CNFZ, located on the western boundary of the Taiwan Strait, is 450 km in length and ~40 km in width (Xu et al. 2006). It formed during the Late Cretaceous and controlled the development of the extensional structure of the CRSC and Taiwan Strait during the Cenozoic, therefore affecting the distributions of geothermal anomalies, volcanic activity, and dynamic metamorphic zones. The CNFZ is an important seismic zone and is currently active. There are five main NW striking active faults, i.e. Minjiang faults, Shaxian-Nanao faults, Yongan-Jinjiang faults, Jiulongjiang faults, and Shanghang-Zhaoan faults respectively, from north to south in the study region (Fig. 10B) that produce a heterogeneous stress field and differential crustal deformation. Furthermore, in the CRSC, NW-striking faults are mainly strike-slip faults, which control the development of basins, plains, and bays in coastal areas. It is worth noting that the faults north of the Yongan-Jinjiang fault are all dextral

strike-slip, while the faults south of the Jiulongjiang fault are all sinistral strike-slip. The JM-1 borehole, located in Xiamen City, is in the transition area. The NE and NW striking faults intersect and cut across each other geographically and tectonically. This produces multiple consequences that have not only affected the basin growth and geothermal distribution but have also dominated the seismic activity of the neighboring regions. The BFZ is a seismogenically strong fault zone that has produced or controlled several destructive historical earthquakes ( $M \geq 7$ ) (Xu et al. 2006). In contrast, the CNFZ is seismically weaker than the BFZ in intensity, frequency, and spatial density. It has been statistically shown that most small to moderate ( $M \leq 5$ ) earthquakes in the CNFZ occur at relatively shallow depths ( $< 15$  km) (Xu et al. 2006). Our ASR stress measurements were conducted in the JM-1 borehole, which is located near the Zhangzhou Basin and is only several kilometers from a secondary fault of the 110 km long, NW striking Jiulongjiang fault zone.

According to compiled stress data (Fig. 10B), in the CRSC, from north to south, the horizontal principal stress direction has undergone a significant but smooth transition from NNW to NWW in a counterclockwise manner. The stress directions change as largely as  $\sim 60^\circ$ . Overall, this change is consistent with orientation changes of focal mechanisms, regardless of the earthquake type, reflecting a stable regional active tectonics.

#### 5.4 Implications for Geothermal Resources Development in the Future

Geophysical surveys have shown that there may be considerable dry hot rock resources in the crystalline rocks of the shallow crust in the Xiamen region (Lin et al. 2020). The development of hot dry rock relies on hydraulic fracturing technology to create a large-scale fracture network in the high-temperature and low-permeability reservoir to improve the hydraulic conductivity of the rock mass, and then extract heat energy for power generation. Hydraulic fracturing needs to utilize and reactivate the pre-existing natural fractures to establish stable hydraulic channels with various (artificial and natural) fractures. In-situ stress characteristics play a major role in hydraulic fracturing design and field operation (Valley and Evans 2019).

Those natural fractures that align favorably with the present-day stress field, contribute to subsurface fluid flows. Generally, hydraulic fractures propagate in the  $S_{Hmax}$  direction because they open and dilate with minimal energy consumption against the minimum principal stress (Zoback 2007). Therefore, both the orientation and regime of the in-situ stress in the geothermal reservoir are imperative before drilling to optimize well performance. The results of ASR stress measurements indicate that the stress regime is normal faulting in the Xiamen region. In this case, the  $\sigma_3$  is

horizontal and equals to  $S_{hmin}$ , which would result in the development of vertical hydraulic fractures and preferential opening/stimulation of sub-vertical pre-existing fractures as opposed to horizontal ones. The ASR results show that the regional  $S_{Hmax}$  direction is  $N43^\circ \pm 19^\circ W$ . Hence, the vertical hydraulic fractures would propagate parallel to this direction.

Furthermore, for hot dry rock reservoirs with a normal faulting stress regime, deviated drilling is necessary and effective to enhance productivity. However, wellbore instability issues, typically manifested as wellbore breakouts and collapses, are common in the development process and can cause vast increases in deviated drilling costs (Zoback et al. 2007). The in-situ stress state can be used to evaluate the risk of wellbore stability. In this study, the normal faulting stress regime ( $S_v > S_{Hmax} > S_{hmin}$ ) is estimated to be dominant in the deep reservoir of hot dry rock, and the largest differential stress comes from between  $S_v$  and  $S_{hmin}$ . As a result, wells that deviated parallel to the  $S_{Hmax}$  orientation may encounter wellbore instability problems in the reservoir. Due to the lack of imaging logging data, the development of the wellbore breakouts of the JM-1 borehole remains unclear. However, as discussed above, the differential stresses between the three principal stresses are relatively low. Therefore, although laboratory tests have shown that the compressive strength of the granite from the JM-1 borehole is relatively weak, the extent of wellbore collapse in the deep reservoir may not necessarily be severe. It can be reasonably expected that in future drilling, it is not necessary to use high-density mud as the drilling circulating fluid to effectively mitigate or even avoid the problem of wellbore instability.

To quantitatively understand and analyze the influence of in-situ stress state on natural fractures during hydraulic fracturing operations, the Mohr–Coulomb failure criterion is here introduced to evaluate the tendency of natural fracture reactivations in the Xiamen region. Usually, the hot dry rock is developed economically at 4–6 km depth. For simplicity, we mainly study the reactivity of natural fractures at 5 km depth of dry hot rock reservoirs in the Xiamen region. The in-situ stress state is determined by linear extrapolation according to the measured results of the JM-1 borehole (Fig. 8). The static groundwater level of the JM-1 borehole is 200 m, and the initial pore pressure of 5 km can be assumed to be 48 MPa. The coefficient of friction of natural fractures is 0.6. Here, the string friction during hydraulic fracturing and the cohesion of natural fractures are not considered.

It can be seen that all the natural fractures are generally stable under the present-day in-situ stress state (Fig. 11). However, pore pressure is increasing with the injection of fluids into the reservoir rocks, which results in the leftward movement of Mohr's Circle and increases the possibility of being reactivated for natural fractures. When the injection pressure reaches 7.6 MPa, the natural fractures that are at the

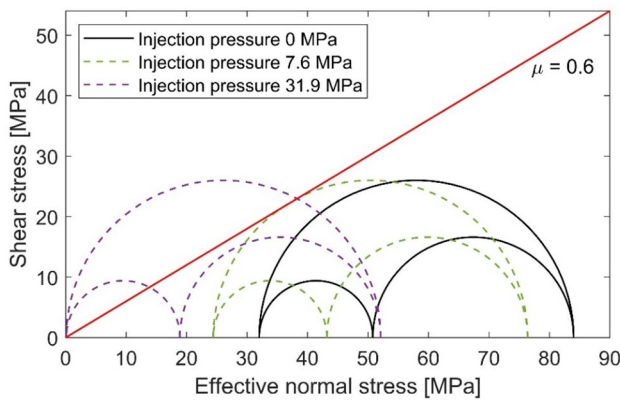


**Fig. 11** Quantitative influence of in-situ stress state on the possibility of reactivation of natural fractures under different injection pressures in hot dry rock reservoirs in the Xiamen region

optimal directions with the maximum principal stress will be in a critical stress state (Eq. (5)). When the injection pressure exceeds 31.9 MPa, some natural fractures will overcome the minimum horizontal principal stress and be in a state of tensile failure. However, this scenario needs to be avoided in the development of hot dry rock. Therefore, the critical pore pressures for reactivation of natural fractures caused by fluid injection are between 7.6 and 31.9 MPa (see Fig. 11). It is objectively evaluated that the stimulation pressure of hot dry rock reservoir in the Xiamen region is not high and is relatively suitable for development in the future.

## 6 Conclusions

To better understand the stress state of the shallow crust in the CRSC, the ASR method and related laboratory tests were employed to constrain the full stress tensors at ~2 km depth in a granite borehole in Xiamen city. Rock mechanics and ASR compliance experiments were conducted to help constraint the in-situ stress state.

- (1) The results show that from ~1865 to ~1959 m in depth, the  $S_{Hmax}$  and  $S_{hmin}$  are 36.1–48.7 MPa and 34.0–38.5 MPa, respectively. The three-dimensional principal stresses are characterized by  $S_v > S_{Hmax} > S_{hmin}$ , showing that the shallow crust is controlled by the normal-faulting stress state, as well as indicating the domination of the vertical stress and the presence of an extensional environment in the CRSC.
- (2) Paleomagnetic tests show that the orientation of the  $S_{Hmax}$  is  $N43^\circ \pm 19^\circ W$ , which is consistent with the borehole breakouts information as well as the absolute plate motion of the Philippine Sea plate, indicating that

the convergence and compression of the Eurasian and Philippine Sea plates play a first-order role in controlling the crustal stress patterns.

- (3) The frontal collision between large tectonic plates usually produces high compressive stress accumulations near the margins. However, our ASR stress measurement results and borehole imaging data show that there is a lower horizontal compressive stress state in the shallow crust in the CRSC (especially in Xiamen City).
- (4) In particular, the significance of in-situ stress for the future development of hot dry rock resources in the Xiamen region is appropriately discussed. Based on the present-day in-situ stress state, the reactivation possibility of natural fractures under different injection pressures is quantitatively analyzed. Generally, the critical injection pressures for reactivation of optimally-oriented natural fractures are between 7.6 and 31.9 MPa. Therefore, the operation of hydraulic fracturing in hot dry rock reservoirs is relatively easy, and its effects on the reservoir environment may be safe and clear.

**Acknowledgements** This study was financially supported by research funds from the National Natural Science Foundation of China (Nos. 42177175, 41807222, 41702351), the China Geological Survey Project (DD20221660, DD20190138), and the CGS Research Fund (No. DZLXJK201706). Dr. Dongsheng Sun assisted in ASR measurement equipment and analysis software. Dr. Junling Pei helped conducted the paleomagnetic test of the ASR cores. Many thanks to Prof. Guiling Wang and Dr. Wenjing Lin for their help in the stress investigation in the JM-1 borehole. Dr. Haonan Gan provided geological data and rock cores of the JM-1 borehole. Particularly, the first author would thank Mr. Sho Nagata for helping conduct the ASR compliance experiment at Kyoto University. The original draft was edited by Elsevier Language Editing Services. Thanks to Dr. Ke Gao and Dr. Yu Feng for helping to improve the language of the revised manuscript.

**Author contribution** Chongyuan Zhang: methodology, formal analysis, writing–review editing. Weiren Lin: Formal analysis, writing–review editing; Manchao He: validation, writing–review editing; Zhigang Tao: Formal analysis, writing – review editing; Wen Meng: Formal analysis.

## Declarations

**Conflict of interest** The authors declare that they have no known competing financial interests or personal relationships that could have appeared to influence the work reported in this paper.

## References

- Anderson EM (1951) The dynamics of faulting and dyke formation with application to Britain. Oliver and Boyd, Edinburgh
- Ask D, Stephansson O, Cornet FH et al (2009) Rock stress, rock stress measurements, and the integrated stress determination method (ISDM). *Rock Mech Rock Eng* 42:559. <https://doi.org/10.1007/s00603-009-0058-9>

- Byrne TB, Lin W, Tsutsumi A et al (2009) Anelastic strain recovery reveals extension across SW Japan subduction zone. *Geophys Res Lett* 36(23):L01305. <https://doi.org/10.1029/2009GL040749>
- Calais E, Vergnolle M, San'kov V et al (2003) GPS measurements of crustal deformation in the Baikal-Mongolia area (1994–2002): Implications for current kinematics of Asia. *J Geophys Res* 108:2501
- Carpenter BM, Marone C, Saffer DM (2011) Weakness of the San Andreas Fault revealed by samples from the active fault zone. *Nat Geosci* 4:251–254
- Collettini C, Tesei T, Scuderi MM et al (2019) Beyond Byerlee friction, weak faults and implications for slip behavior. *Earth Planet Sci Lett* 519:245–263
- Cui J, Lin W, Wang L et al (2014) Determination of three-dimensional in situ stresses by anelastic strain recovery in Wenchuan Earthquake Fault Scientific Drilling Project Hole-1 (WFS-D-1). *Tectonophysics* 619:123–132
- Eberhardt E, Stead D, Stimpson B et al (1998) Identifying crack initiation and propagation thresholds in brittle rock. *Can Geotech J* 35:222–233
- Eberhardt E, Stimpson B, Stead D (1999) Effects of grain size on the initiation and propagation thresholds of stress-induced brittle fractures. *Rock Mech Rock Engng* 32:81–99
- Gao Y, Wu J, Cai JA et al (2009) Shear-wave splitting in the southeast of Cathaysia block, South China. *J Seismolog* 13:267–275
- Gao L, Lin W, Sun D et al (2014) Experimental anelastic strain recovery compliance of three typical rocks. *Rock Mech Rock Eng* 47:1987–1995
- Heidbach O, Rajabi M, Cui X et al (2018) The World Stress Map database release 2016: Crustal stress pattern across scales. *Tectonophysics* 744:484–498
- Horii H, Nemat-Nasser S (1985) Compression-induced microcrack growth in brittle solids: axial splitting and shear failure. *J Geophys Res* 90:3105–3125
- Hu X, Zang A, Heidbach O et al (2017) Crustal stress pattern in China and its adjacent areas. *J Asian Earth Sci* 149:20–28
- Huang HH, Wu YM, Song X et al (2014) Investigating the lithospheric velocity structures beneath the Taiwan region by nonlinear joint inversion of local and teleseismic P wave data: Slab continuity and deflection. *Geophys Res Lett* 41:6350–6357
- Jaeger JC, Cook NGW (1979) *Fundamentals of rock mechanics*. Chapman & Hall, New York
- Li S, Santosh M, Zhao G et al (2012) Intracontinental deformation in a frontier of super-convergence: a perspective on the tectonic milieu of the South China Block. *J Asian Earth Sci* 49:313–329
- Li R, Chen QC, Zhang CY et al (2016) In Situ Stress Characteristics In The Western Coast Of Taiwan Strait. *Acta Geol Sin* 90:1703–1714 (in Chinese)
- Li J, Zhang Y, Zhao G et al (2017) New insights into Phanerozoic tectonics of South China: early Paleozoic sinistral and Triassic dextral transpression in the east Wuyishan and Chencai domains, NE Cathaysia. *Tectonics* 36:819–853
- Li P, Ren F, Cai M et al (2019) Present-day stress state and fault stability analysis in the capital area of China constrained by in situ stress measurements and focal mechanism solutions. *J Asian Earth Sci* 185:104007
- Lin W, Kwaśniewski M, Imamura T et al (2006) Determination of three-dimensional in situ stresses from anelastic strain recovery measurement of cores at great depth. *Tectonophysics* 426:221–238
- Lin W, Yeh EC, Ito H et al (2007) Preliminary results of stress measurement using drill cores of TCDP Hole-A: an application of anelastic strain recovery method to three-dimensional in-situ stress determination. *Terr Atmos Ocean Sci* 18:379
- Lin S, Ding X, Chen W et al (2009) Research on focal mechanism solutions and tectonic stress field in Fujian region. *J Geodesy Geodyn* 29(5):27–32
- Lin W, Chen X, Gan H et al (2020) Geothermal, geological characteristics and exploration direction of hot dry rocks in the Xiamen bay- Zhangzhou basin, southeastern China. *Acta Geol Sin* 94(7):2066–2077
- Liu M, Stein S, Wang H (2011) 2000 years of migrating earthquakes in north china: how earthquakes in midcontinents differ from those at plate boundaries. *Lithosphere* 3:128–132
- Ma X (1989) *Lithospheric dynamics atlas of China*. China Cartographic Publishing House, Beijing
- Matsuki K (2008) Anelastic strain recovery compliance of rocks and its application to in situ stress measurement. *Int J Rock Mech Min Sci* 45:952–965
- Matsuki K, Takeuchi K (1993) Three-dimensional in situ stress determination by anelastic strain recovery of a rock core. *Int J Rock Mech Min Sci Geomech Abstr* 30:1019–1022
- Matsuki K (1991) Three-dimensional in-situ stress measurement with anelastic strain recovery of a rock core. In: Wittke W (ed.), *Proceedings of the 7th International Congress on Rock Mechanics*. Taylor and Francis, London, pp. 557–560
- Molnar P, Gipson JM (1996) A bound on the rheology of continental lithosphere using very long baseline interferometry: The velocity of south China with respect to Eurasia. *J Geophys Res Solid Earth* 101(B1):545–553
- Oikawa Y, Yamaguchi T (2000) Stress measurement using rock core in an HDR field. In *Proceedings World Geothermal Congress 2000*. Kyushu-Tohoku, Japan
- Oohashi K, Lin W, Wu HY et al (2017) Stress state in the Kumano Basin and in slope sediment determined from Anelastic strain recovery: results from IODP Expedition 338 to the Nankai trough. *Geochem Geophys Geosyst* 18:3608–3616
- Ranjbar-Karami R, Rajabi M, Ghavidel A et al (2019) Contemporary tectonic stress pattern of the Persian Gulf Basin Iran. *Tectonophysics* 766:219–231
- Shen ZK, Zhao C, Yin A et al (2000) Contemporary crustal deformation in east Asia constrained by Global Positioning System measurements. *J Geophys Res Solid Earth* 105(B3):5721–5734
- Sun D, Sone H, Lin W et al (2017) Stress state measured at ~7 km depth in the Tarim Basin, NW China. *Sci Reports* 7:4503
- Teufel LW (1983) Determination of in situ-stress from anelastic strain recovery measurements of oriented cores. *Symp. SPE/DOE* 11649, Denver; 421–430
- Tezuka K, Niitsuma H (2000) Stress estimated using microseismic clusters and its relationship to the fracture system of the Hijiori hot dry rock reservoir. *Eng Geol* 56:47–62
- Valley B, Evans KF (2019) Stress magnitudes in the Basel enhanced geothermal system. *Int J Rock Mech Min Sci* 118:1–20
- Wang B, Sun D, Chen Q et al (2020) Stress-state differences between sedimentary cover and basement of the Songliao Basin, NE China: In-situ stress measurements at 6–7 km depth of an ICDP Scientific Drilling borehole (SK-II). *Tectonophysics* 777:228337
- Wolter KE, Berckhemer H (1989) The time dependent strain recovery is investigated for drill cores of two rock types from the German Continental Deep Drilling Project (KTB). *Rock Mech Rock Eng* 22:273–287
- Wu M, Zhang C, Fan T (2016) Stress state of the Baoxing segment of the southwestern Longmenshan Fault Zone before and after the Ms 7.0 Lushan earthquake. *J Asian Earth Sci* 121:9–19
- Xie FR (ed) (2015) *Recent tectonic stress map of China and its adjacent areas*. Sinomaps Press, Jiangsu
- Xu ZH, Xu GQ et al (1999) Present-day tectonic stress in the East China Sea region and its possible origin. *Acta Seismol Sin* 12:542–549
- Xu H, Qiu X, Zhao M et al (2006) Characteristics of the crustal structure and hypocentral tectonics in the epicentral area of Nan'ao earthquake (M7.5), the northeastern South China Sea. *Chin Sci Bull* 51(2):95–106



- Yamamoto Y, Lin W, Oda H et al (2013) Stress states at the subduction input site, Nankai Subduction Zone, using anelastic strain recovery (ASR) data in the basement basalt and overlying sediments. *Tectonophysics* 600:91–98
- Yin TB, Shu RH, Li XB et al (2016) Comparison of mechanical properties in high temperature and thermal treatment granite. *Trans Nonferrous Metals Soc China* 26:1926–1937
- Zang A, Berckheimer H (1993) Classification of crystalline drill cores from the KTB deep well based on strain, velocity and fracture experiments. *Int J Rock Mech Min Sci* 30(4):331–342
- Zang A, Stephansson O (2010) *Stress field of the earth's crust*. Springer, Netherlands
- Zang A, Berckheimer H, Lienert M (1996) Crack closure pressures inferred from ultrasonic drill-core measurements to 8 km depth in the KTB wells. *Geophys J Int* 124(3):657–674
- Zhang PZ, Deng QD, Zhang ZQ et al (2013) Active faults, earthquake hazards and associated geodynamic processes in continental China. *Sci Sinica Terrae* 43:1607–1620
- Zhang P, Hu QY, Feng CJ et al (2015) Present in-situ stress measurement in middle segment of Changle-Nan'ao Fracture Belt along the Western Coastal Region of Taiwan Strait and an Analysis of Its Activity. *Acta Geosci Sin* 36:483–490
- Zhang C, Chen Q, Qin X et al (2017) In-situ stress and fracture characterization of a candidate repository for spent nuclear fuel in Gansu, northwestern China. *Eng Geol* 231:218–229
- Zhang Y, Yao H, Yang HY et al (2018) 3-D crustal shear-wave velocity structure of the Taiwan Strait and Fujian, SE China, Revealed by Ambient Noise Tomography. *J Geophys Res Solid Earth* 123:8016–8031
- Zhao GC, Cawood PA (2012) Precambrian geology of China. *Precambrian Res* 222:13–54
- Zhou SY, Wu Y, Qin XJ et al (2000) Crustal horizontal movement in Fujian and its neighboring sea region from 1994 to 1997 based on Multi-Scale GPS Surveying Data. *Chin J Geophys* 43:504–531
- Zoback ML (1992) First-and second-order patterns of stress in the lithosphere: The World Stress Map Project. *J Geophys Res* 97(8):11703–11728
- Zoback MD (2007) *Reservoir geomechanics*. Cambridge University Press, Cambridge

**Publisher's Note** Springer Nature remains neutral with regard to jurisdictional claims in published maps and institutional affiliations.